PROCEEDINGS OF THE ROYAL SOCIETY B

CrossMark click for updates

Proc. R. Soc. B (2012) **279**, 3041–3048
doi:10.1098/rspb.2012.0335
Published online 11 April 2012

Biomineral ultrastructure, elemental constitution and genomic analysis of biomineralization-related proteins in hemichordates

C. B. Cameron[1,*] and C. D. Bishop[2]

[1]*Département de Sciences Biologiques, Université de Montréal, C.P. 6128, Succ. Centre-ville, Montréal, Quebec, Canada H3C 3J7*

[2]*Department of Biology, St Francis-Xavier University, 2320 Notre Dame Avenue, Antigonish, Nova Scotia, Canada B2G 2W5*

Here, we report the discovery and characterization of biominerals in the acorn worms *Saccoglossus bromophenolosus* and *Ptychodera flava galapagos* (Phylum: Hemichordata). Using electron microscopy, X-ray microprobe analyses and confocal Raman spectroscopy, we show that hemichordate biominerals are small $CaCO_3$ aragonitic elements restricted to specialized epidermal structures, and in *S. bromophenolosus*, are apparently secreted by sclerocytes. Investigation of urchin biomineralizing proteins in the translated genome and expressed sequence tag (EST) libraries of *Saccoglossus kowalevskii* indicates that three members of the urchin MSP-130 family, a carbonic anhydrase and a matrix metaloprotease are present and transcribed during the development of *S. kowalevskii*. The SM family of proteins is absent from the hemichordate genome. These results increase the number of phyla known to biomineralize and suggest that some of the gene-regulatory 'toolkit', if not mineralized tissue themselves, may have been present in the common ancestor to hemichordates and echinoderms.

Keywords: hemichordate; biomineralization; aragonite; skeletal evolution

1. INTRODUCTION

Shells, carapaces, spines, ossicles, spicules and bone have been widely investigated by palaeontologists, physical chemists, material scientists and medical researchers under the common rubric of biomineralization since the late nineteenth century. There are so many minerals formed and so many morphologies produced that common threads connecting basic structures in different taxa are of considerable interest. Biomineralized tissues are the principal source of direct evidence for the ancestry of life on the Earth [1,2], are a rich source of morphological data that inform evolutionary hypotheses [3,4] and represent a remarkable interface between inorganic and organic worlds [5–9]. The generation of biominerals has been the subject of considerable theoretical and mechanistic exploration among the vertebrates, arthropods, molluscs and corals.

Among the invertebrate deuterostomes, biominerals have been reported to exist widely in tunicates [10] and echinoderms [8,9,11]. The oldest deuterostome fossils are the skeletal plates, or ossicles, of stylophoran echinoderms that appeared about 510 Ma [11]. Echinoderm ossicles are composed of numerous, single-calcite crystals that lie on the same crystal axis [6]. This skeletal tissue called stereom [3,12] forms intracellularly or extracellularly and is usually perforated by a network of mesh-like cavities. Morphologically, echinoderm ossicles form an endoskeleton, produced by mesenchymal cells and are usually covered by epidermis [4]. The majority of ossicles function in protection, positioned just under or within the ectoderm.

In sea urchins, ossicle minerals are occluded by secreted proteins that control the growth and physical properties of the material [4,5,13]. Some of these proteins are members of small gene families, which, at least in the purple sea urchin *Strongylocentrotus purpuratus*, are tightly clustered on the genome, suggesting that they expanded relatively recently by gene duplication [14]. Many of these proteins probably arose from ancestral C-lectin domain-containing proteins [14] (including the SM30 and SM50 families of proteins). Other, distantly related proteins, including the MSP-130 family of proteins, matrix metalloproteases and carbonic anhydrases are also implicated in urchin biomineralization. To what extent these molecules may be shared in the other echinoderm classes is poorly known [15] and in hemichordates is unknown.

Here, we provide the first description of biomineralized tissues from hemichordates, including their ultrastructure, and elemental constitution. Second, we searched for sea urchin biomineralization-related proteins in the hemichordate *Saccoglossus kowalevskii* genome. Third, we sought to shed some light on the possible evolutionary relationships between biominerals in echinoderms and hemichordates.

2. MATERIAL AND METHODS

(a) *Specimen collection*

Saccoglossus bromophenolosus were collected in the mud adjacent to the Darling Marine Laboratory (University of

* Author for correspondence (c.cameron@umontreal.ca).

Electronic supplementary material is available at http://dx.doi.org/10.1098/rspb.2012.0335 or via http://rspb.royalsocietypublishing.org.

Received 16 February 2012
Accepted 20 March 2012

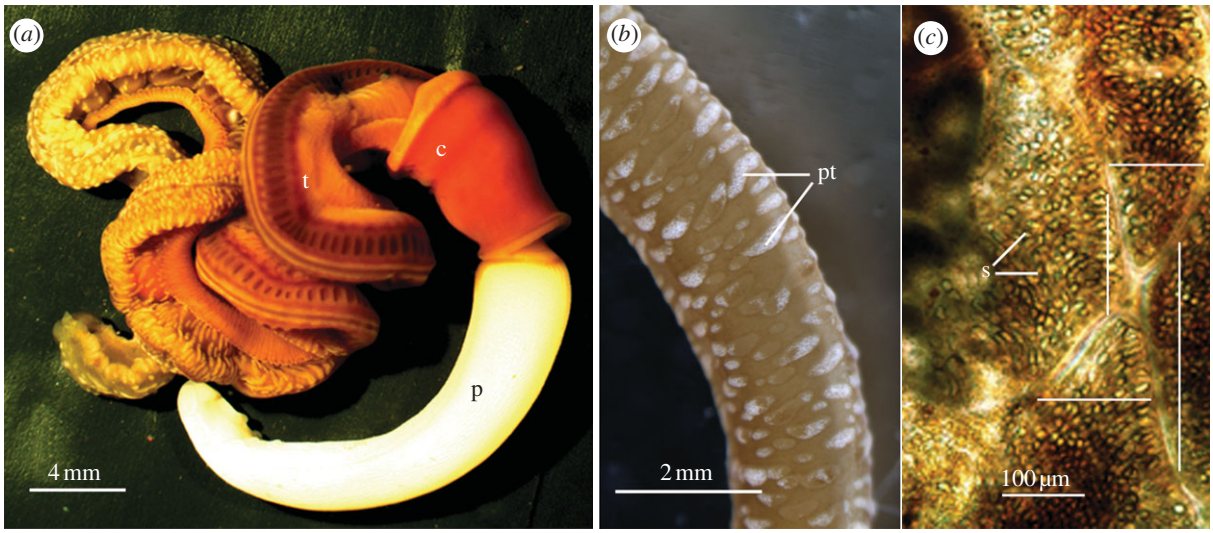

Figure 1. (*a*) Light micrographs of *S. bromophenolosus*. (p, anterior proboscis; c, central collar; t, posterior trunk). (*b*) The trunk is spotted with numerous elevated white protuberances (pt, protuberances). (*c*) Four abutting protuberances located in the groove between the dorsolateral gonads and the ventral midline. Each protuberance is composed of several superficial and transparent spaces, some of which contain a single ossicle (s, spaces). Each of the four lines crosses a single protuberance at one of its narrower termini.

Maine) in September 2008 and *Ptychodera flava galapagos* were collected in sand by S. A. Earl on Florena Island, Galapagos in December 2003.

(b) *X-ray microprobe analyses and scanning electron microscopy*

Ossicles were cleaned in 5 per cent NaOCl for 1 h, washed in several changes of distilled water and transferred to an aluminium SEM stub, carbon-coated (Devon D205A sputter coater), analysed and imaged using a JEOL 8200 Superprobe electron microprobe, with an accelerating voltage of 15 kV, beam current of 20 nA and a spot size of 1 µm. Semi-quantitative X-ray microprobe analyses were done in electron-dispersive spectrometer (EDS) mode. Quantitative analyses were done in wavelength-dispersive spectrometer (WDS) mode, with standards and background X-ray counts analysed every 40 samples. Count times were 20 s and 10 s for peaks and backgrounds, respectively. Matrix corrections were done using the ZAF method and analytical results reported as equivalent weight per cent oxides. The following elements were analysed and calibrated against their respective primary standards (diffraction crystal used in brackets): P (PETJ)-Apatite; Ba (PETJ)-Barite; Na (TAPH)-Jadeite; Si (TAP)-Sanidine; Mn (divalent) (LIFH)-Pyrolusite; K (PETJ)-Sanidine; S (PETJ)-Pyrr_239; Mg (TAPH)-Dolomite; Sr (TAP)-Celestite; Fe (divalent)(LIFH)-Garnet12442; Ca (PETJ)-Dolomite. Primary standards were from the American Society for Testing and Materials (ASTM) or the National Institute of Standards and Technology (NIST). Oxygen was calculated for each analysis on the basis of stoichiometry. For SEM analyses, ossicles were viewed on a Hitachi FE-SEM, model S-4700 with 10 kV acceleration voltage.

(c) *Confocal Raman spectroscopy*

Confocal Raman spectra were acquired with a Renishaw InVia Raman microspectrometer equipped with a deep depletion CCD detector, 1800 l mm^{-1} grating and a holographic notch filter. Excitation was provided using a Spectra Physics argon ion 514.5 nm laser with 28 mW output and 5 mW at the sample. The spectrometer was attached to a Leica microscope with a 50X objective in a 180° backscatter collection configuration.

(d) *Transmission electron microscopy*

For transmission electron microscopy (TEM), *S. kowelvskii* specimens were fixed in 2.5 per cent glutaraldehyde, postfixed in 1 per cent osmium tetroxide, dehydrated and embedded in Epon 812. Ultrathin sections were stained with uranyl acetate and lead citrate and viewed on a Tecnai-12 TEM at 80 kV. We have no TEM data on *Ptychodera* because animals were damaged on collection, then fixed in 4 per cent formaldehyde and later transferred to alcohol.

(e) *Informatics*

See the electronic supplementary material.

3. RESULTS

(a) *Ossicle location, morphology and cellular environment*

The enteropneust *S. bromophenolosus* (figure 1*a*) and the distantly related *P. flava galapagos* (not shown) contain in their epidermis numerous elevated protuberances that appear white (figure 1*b*). In *S. kowalevskii* anterior trunk, the protuberances are located in the grooves between the dorsal midline and the dorso-lateral gonads, and in the groove between the dorso-lateral gonads at the ventral midline (figure 1*a*). They are most abundant and well developed in the posterior intestinal trunk (figure 1*b*). Individual protuberances are composed of numerous fluid-filled vesicles (figure 1*c*) that are elliptical to ovoid and often pointed at the apical end. The vesicles measure 26 µm (mean of +8, $n = 22$) in depth and 15 µm (+5, $n = 25$) in width and the number of vesicles within a protuberance varies widely from 1 to 176 (75 + 65, $n = 9$). An individual vesicle may contain one or no ossicles. Trunk epidermal protuberances are found among the three major enteropneust families, including *S. kowalevskii* [16] (Family: Harrimanniidae), *Spengelia alba* [17] (Family: Spengeliidae), *Ptychodera flava laysanica*, *P. flava*

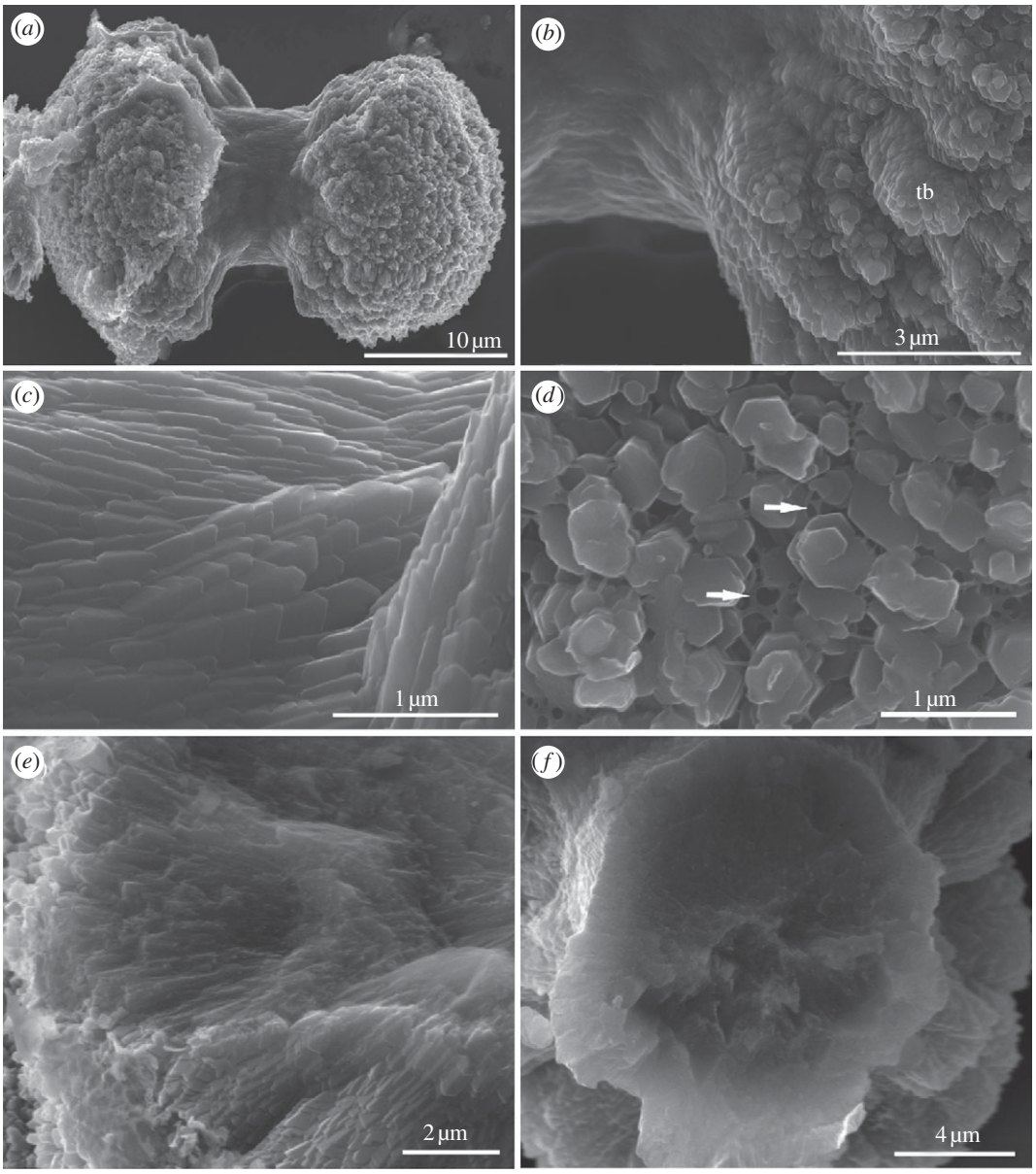

Figure 2. Scanning electron micrographs of ossicles isolated from *S. bromophenolosus* trunk epithelium. (*a*) Lateral view of a typical ossicle. The arrangement and shape of crystals differ between the central shaft and the termini. (*b*) Higher magnification of a terminus showing polycrystalline aggregates that form highly ordered, closely packed, expanding columns or trabeculae, of plate-like crystals (tb, trabeculae). (*c*) Higher magnification view showing the overlapping, smooth and laminar layers that constitute the central shaft portion of the ossicle in (*a*). (*d*) Terminal view of an ossicle, showing the arrangement of trabeculae, the perforated network of holes and a net-like matrix (arrows). (*e*) View of the inside of a fractured terminus. (*f*) View of the inside of a broken shaft.

caledoniensis [18] and *Glossobalanus ruficollis* [17] (Family: Ptychoderidae) suggesting that ossicles may be a general feature of the Enteropneusta.

Although varied in structure, most *S. bromophenolosus* ossicles have a double-ended broccoli-like shape with a central shaft and flared tips (figure 2*a*). Larger ossicles are 30 µm in length, 10 µm across the narrow stalk and 20 µm across the widest point of the flared tips. The tips appear to be polycrystalline aggregates that form highly ordered, closely packed, expanding columns, or trabeculae, of plate-like crystals (figure 2*b*). The shaft region is also highly ordered and closely packed, but smooth and composed of overlapping laminar layers (figure 2*c*). Viewed terminally, the tips of the ossicles are perforated by a network of holes (figure 2*d*), interlaced with a net-like matrix (figure 2*d*, arrows). Internally, the ossicles are solid (figure 2*e*,*f*), similar to the narrow spicules of pluteus larvae [19] or small ossicles of holothuroid adults [20].

Ptychodera flava galapagos ossicles are smaller and much less abundant in the tissue than those of *S. bromophenolosus*. Ossicles are spherical with a mean diameter of 23.46 µm (± 8.38, $n = 20$) and approximately 20 ossicles were isolated from a patch of epidermis measuring 4 mm by 4 mm. On the surface, they are smooth to rugose (figure 3). Ossicles that were fractured revealed an inner core that is porous, though not reminiscent of stereom (figure 3*c*). There are no crystalline plates or layers besides the outer spherical layer.

Hemichordate ossicles are positioned under or within a ciliated epidermis and are enveloped by sclerocyte cells in *Saccoglossus* (figure 4*a*). The cell cytoplasm is

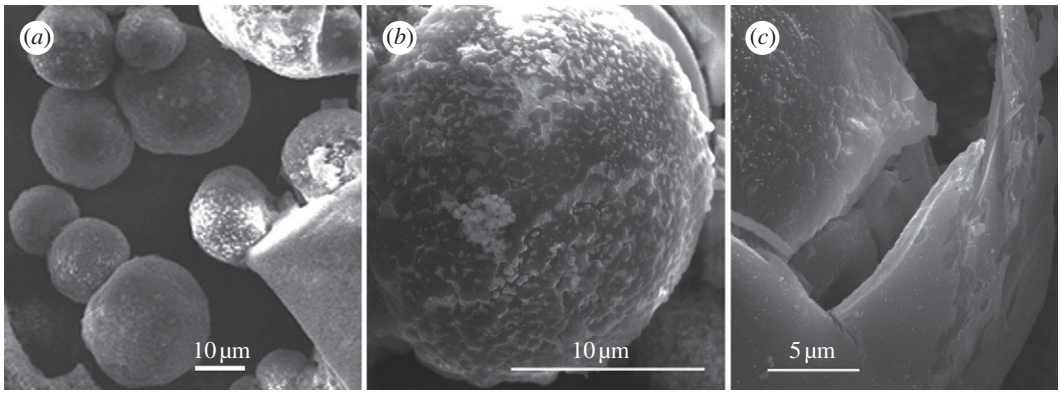

Figure 3. Scanning electron micrographs of ossicles from the trunk epidermis of *Ptychodera flava galapagos*. (*a*) Ossicles are spherical with a mean diameter of 23.46 µm (±8.38, $n = 20$). (*b*) Ossicles are round and rugous. (*c*) They are composed of an outer layer that when fractured reveals a porous interior.

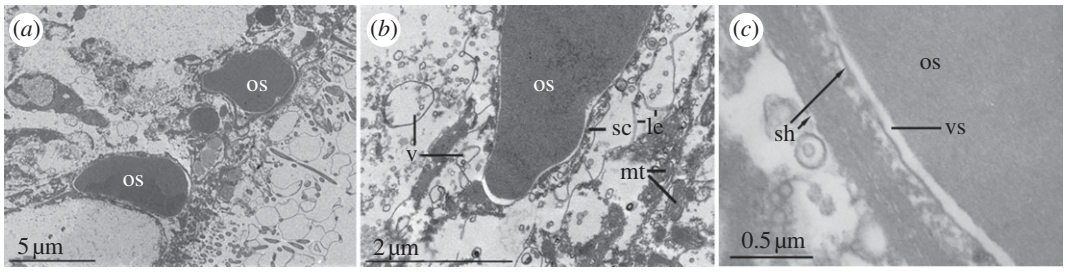

Figure 4. Transmission electron micrographs of sections through the epithelium of *S. bromophenolosus* showing the ossicles and sclerocyte cells. (*a*) The ossicles are positioned in a heavily ciliated epidermis (os, ossicles). (*b*) The border between an ossicle and its surrounding sheath of sclerocytes indicates an extracellular position. The cytoplasm is filled with transparent vesicles and abundant mitochondria (v, vesicles, mt, mitochondria). An electron-dense boundary layer (le, lamina externe) surrounds the cell body. (c) Sclerocyte cells form a sheath around the ossicle (sh, sheath). The inner sheath is lined with matrix material that presumably crosses the vacuolar space to be incorporated in the ossicle (vs, vacuolar space).

characterized by abundant vacuoles and mitochondria. The sclerocyte cell bodies are surrounded by an electron-dense boundary layer (lamina externa; figure 4*b*), which is not present in non-sclerocytes [3,21]. There is an electron-transparent space between the enveloping sheath of sclerocytes and the growing mineral surface (figure 4*c*). This cavity may be derived from cell vacuoles where the mineral is deposited extracellularly. In sea urchins, this space may be sealed off from the surrounding area to maintain a fluid-filled cavity of the necessary ionic composition and pH around the growing surface [3,22].

(b) *Elemental constitution of ossicles*

The elemental constitution of isolated ossicles was determined by X-ray microprobe analyses. Energy-dispersive analysis (using EDS) identified calcium, oxygen and carbon as principal elements (figure 5*a*). Wave-dispersive analysis quantified calcium and less-abundant elements identified by EDS (figure 5*b*), confirming that *S. bromophenolosus* and *P. flava galapagos* ossicles are composed of $CaCO_3$ and minor (approx. 1%) quantities of strontium and magnesium.

Because $CaCO_3$ crystals can take the form of vaterite, aragonite or calcite, *S. kowalevskii* ossicles were subjected to confocal Raman spectroscopy to distinguish between these crystal polymorphs. Spectra collected from six haphazardly chosen ossicles exhibited peaks at 156 and 206 cm^{-1}, a small peak at 708 cm^{-1} and a strong peak at 1086 cm^{-1} (figure 5*c*), which is characteristic of aragonite [23]. Exhaustive line map and depth scans at 1 µm resolution generated no evidence of a calcite peak at 285 cm^{-1}. In contrast, Raman spectra collected from a sea urchin ossicle that clearly correspond to calcite (figure 5*c*). Although nitrogen was not detected by EDS analysis, protease treatment disintegrated the ossicles suggesting that they possess a protein matrix.

(c) *Informatics*

The genome of the hemichordate *S. kowalevskii*, sister taxon to *S. bromophenolosus*, contains homologues of five of 10 of the signalling molecules and extracellular matrix proteins involved in echinoderm biomineralization (table 1). See the electronic supplementary material for methods. A matrix metalloprotease (electronic supplementary material, figure S1) a carbonic anhydrase (electronic supplementary material, figure S2) and three MSP-130-like proteins (electronic supplementary material, figure S3) were recovered from hemichordate-translated gene sequences. Of the seven known MSP-130 urchin genes, five are expressed in primary mesenchyme cells (PMCs) [14] and are present in urchin test, spine, tooth and spicule [14,24,25]: Sp-Msp130L, Sp-Msp130, Sp-Msp130r1, Sp-Msp130r2, Sp-Msp130r3 (Glean3_entries 06387; 02088; 13822; 16506; 13823, respectively), but for completeness, we have included all known non-redundant urchin Msp130-like sequences [24] in our phylogenetic tree (electronic supplementary material, figure S3). Three homologues of this gene family, which

(*a*)

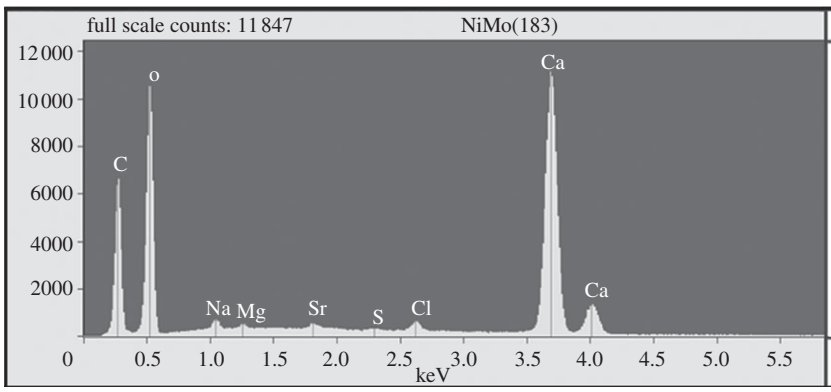

(*b*)

element	X-ray	mean wt, % oxide	s.d.
P	Ka	0.16	0.05
Ba	La	0	0
Na	Ka	0.73	0.33
Si	Ka	0.02	0.02
Mn	Ka	0.02	0.01
K	Ka	0.04	0.01
S	Ka	0.24	0.06
Mg	Ka	0.38	0.17
Sr	La	0.56	0.28
Fe	Ka	0.02	0.02
Ca	Ka	52.84	4.27
total		55.01	

(*c*)

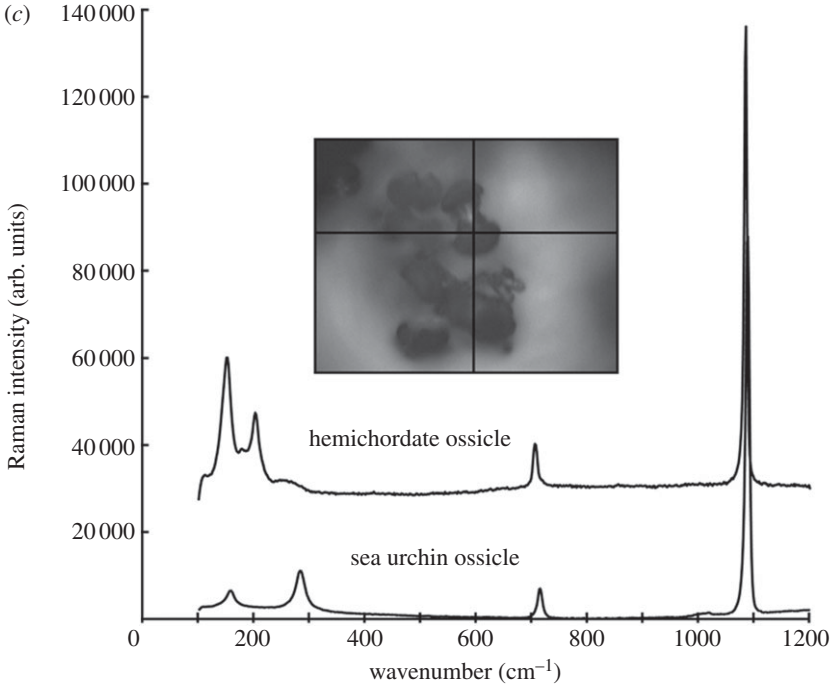

Figure 5. Determination of ossicle elemental constitution using X-ray microprobe analysis and crystal identity using confocal Raman spectroscopy. The ossicles of both species are composed of $CaCO_3$, so only *Saccoglossus* data are shown. (*a*) Representative plot of EDS analysis of the central shaft of a single ossicle. (*b*) WDS analysis on 15 haphazardly chosen ossicles. Quantities are reported as mean weight % oxides. (*c*) Raman spectra for ossicles from *S. bromophenolosus* and a sea urchin test. The inset indicates the position on the hemichordate ossicle from which the spectral data were collected.

we call *S. kowalevskii* MSP-1, 2 & 3 were recovered from both translated genome sequences as well as gastrula and early juvenile EST libraries of *S. kowalevskii*, indicating that the sequences recovered from the translated genomic sequences are transcribed. Significantly, the sister clade to the *S. kowalevskii* MSP130 sequences is composed exclusively of *S. purpuratus* sequences known to be expressed in PMCs. The monophyletic grouping of the three *S. kowalevskii*-translated proteins suggests that a single copy existed in the hemichordate ancestor, and has undergone two duplication events.

Matrix metalloproteinase inhibitors disrupt spicule formation by primary mesenchyme cells in the sea urchin embryo [26]. Four members of this gene family are expressed in all four urchin skeletal matrices and have a homologue in the *S. kowalevskii* genome and EST libraries. This translated protein is most similar to urchin Sp-Mt1-4/MmpL7, Glean3:28748 (tree not shown; electronic supplementary material, figure S1). Carbonic anhydrases are upregulated in the PMCs postgastrulation and localized to the leading edge of the growing larval arms of the urchin *Heliocidaris tuberculata* [27]. One, Sp-Clara7LA (Glean3:12518), is the most abundant in all four proteomically analysed skeletal matrices indicating that it may be required for mineralization in urchins [24]. This same protein has a gene homologue in the *S. kowalevskii* genome and gastrula and early juvenile EST libraries (electronic supplementary material, figure S2). We identified sequences containing C-type lectin domains in the genome of *S. kowalevskii* but bona fide SM proteins were not recovered and thus appear to be unique to urchins.

4. DISCUSSION

The discovery of a new type of biomineral, heretofore unknown in Hemichordata, raises a number of new and interesting research avenues. First, these biominerals are structurally interesting, and present new opportunities for comparisons with known biominerals from other

Table 1. A list of 10 urchin spicule matrix proteins that were found in test, spine, tooth and spicule proteomes [24] and which (at least one member of a family) have been experimentally verified to be involved in urchin biomineralization. Amino acid sequences corresponding to proteins in bold have putative homologues in the *S. kowalevskii*-translated genome and mRNA encoding these sequences are present in *S. kowalevskii* EST libraries. E-values for the three *S. kowalevskii* MSP130s are based on comparison with urchin MSP130rel1.

SpBase	urchin protein ID	*Saccoglossus* subject ID	e-value
SM proteins and other C-type lectin-like domain containing proteins			
SM50	Glean:18811	not present	
PM27	Glean:30147	not present	
SM29	Glean:05990	not present	
SM32	Glean:18810	not present	
SM37	Glean:18813	not present	
SP-Clect_14	Glean:05991	not present	
matrix metalloproteases			
Sp-Mt1-4	Glean:13669/13670	XP_002738586	3e−93
Sp-Mt1-4/5	Glean:28748/28749		
MSP130 proteins			
Sp-Msp130′s	Glean:13821	XP_002739468.1	3e−54
		XP_002733636.1	6e−37
		XP_002739469.1	3e−47
carbonic anhydrases			
Sp-Cara7LA	Glean:12518	XP_002735813	4e−39

taxa. Second, hypotheses of function will need to be advanced and tested to explain the presence of these complex structures; presently, it is unknown how common these biominerals are within the hemichordate phylum, and whether their presence varies seasonally or with life cycle stage. Third, an investigation into the embryonic origin of these biominerals, with particular respect to the germ layers and cellular structures that produce them, is warranted. Fourth, the presence of a biomineral produced in the epidermis of animals that are the sister taxon to echinoderms formally raises the possibility that biomineralization in the Ambulacraria is a homologous feature. Fifth, fossil evidence, in the form of microscopic ossicles, for hemichordate ancestors may be present and worth searching for. We develop these latter two points in some detail.

One clear similarity between echinoderms and hemichordates is the $CaCO_3$ composition of their skeletal elements. In contrast, hemichordate biominerals differ from those of echinoderms in that they are composed of aragonite, rather than the echinoderm polymorph calcite, and they have a lower quantity of magnesium. Notably, vaterite and aragonite can transform into calcite [28], both crystal polymorphs appear in closely related species of coral [5], tunicate [10] and bivalve [7], and are even present together in the bimineralic skeletons of bryozoans [29]. These observations suggest that the developmental pathways that produce $CaCO_3$ polymorphs are similar, if not identical.

Saccoglossus kowalevskii ossicles develop in an extracellular space, and form a polycrystalline aggregate of laminar layers, with perforations that, on the surface, are reminiscent of a poorly developed stereom. This latter structural comparison is less concrete than the elemental one, because the central shaft of hemichordate ossicles is solid and because of the possibility that isolation and preparation of hemichordate ossicles introduced artefacts. The interior core of *P. flava galapagos* ossicles, though porous, does not resemble a stereom. Further work will be required to clarify these potentially informative structural details but, in the main, their homology with ossicles of echinoderms is equivocal.

In sea urchins, biomineralization is regulated by secreted proteins that are closely associated with the mineral element component of the biomineral. The proteins in the sea urchin *S. purpuratus* make only a minor contribution to its biomineral mass [15], but probably play an important role in regulating the growth and physical characteristics of the biomineral. The urchin larval skeleton is produced by the PMCs—a specialized population of embryonic mesodermal cells derived from the large micromere lineage. PMCs express a family of SM proteins, and a family of cell surface proteins consisting of at least five MSP130-related proteins and a matrix metalloproteinase [26] that may function in biomineralization [25,30,31]. Our analysis of the *S. kowalevskii*-translated genome, using 10 sea urchin proteins as queries, revealed five biomineralization genes: three MSP130 genes, a matrix metalloprotease and a carbonic anhydrase. The one urchin carbonic anhydrase probably required for biomineralization [24] is shown with its corresponding *S. kowalevskii* protein sequence (table 1; electronic supplementary material, figure S2). The one matrix metalloprotease is closest to urchin glean3_28748 (Sp-Mt1-4/MmpL7; table 1; electronic supplementary material, figure S1). These genes were also recovered from EST libraries developed from *S. kowalevskii* gastrulae and early juveniles. Illies *et al.* [25] conducted a sequence alignment of five MSP130 genes (three from *S. purpuratus* and one each from *Heliocidaris tuberculata* and *H. erythrogramma*) and found significant variation among those sequences in the presence and length of glycine-rich motifs. Despite the absence in *S. purpuratus* MSP130-related 1 and 2 of significant glycine-rich motifs, those genes are nevertheless annotated as spicule matrix genes because they are expressed at high levels in primary mesenchyme cells. Moreover, despite sharing relatively low overall sequence identity

(in the 30% range), *S. purpuratus* MSP130-related 1 and 2 do unequivocally share short stretches of high sequence identity with MSP130, supporting the homology assignment. None of the three *S. kowalevskii* sequences that we found contains glycine-rich domains and, therefore, this appears to be an innovation of the urchins. By definition then, in *S. kowalevskii*, hits were based on sequence similarity outside this domain, obviating the possibility that, at least in the case of MSP130-like genes, hits were due to shared low-complexity regions. In contrast, SM-like sequences were not recovered and appear to be unique to echinoderms.

Together, these data permit an interpretation of an evolutionary relationship between the genetic programmes of biomineralization in echinoderms and hemichordates. Certainly, some of the genes are present and transcribed, but further study is needed to determine if they are involved in biomineral formation and occluded in acorn worm biomineralized elements.

The oldest echinoderm fossils, the stylophorans, appeared about 510 Ma [11]. Molecular clock data suggest that they are not the oldest echinoderms. Their well-developed stereom, ossicle disparity and body plan asymmetry suggest that they did not appear de novo, but represent a stem-group descendent of an ancestor that more plausibly possessed simpler, smaller and less well-organized ossicles. There is a rich and diverse fossil record of echinoderm skeletal elements [6] including very small Cambrian ossicles [1]. The enteropneust fossil record, by contrast, is poor and comparatively young [32] but further characterization of enteropneust ossicles may shed new light on interpretations of Early Cambrian and Proterozoic microfossils and may support molecular phylogenetic [33,34] and evolutionary developmental assertions [35] that the ancestral deuterostome resembled an enteropneust [33] and, considering the present results, that it possessed biominerals.

Based on our evidence, we cannot reject the hypothesis that biomineralization in the Ambulacraria is homologous at the mineral element, cellular or molecular levels. Model developmental systems such as *S. purpuratus* continue to provide significant new information about biomineralization in echinoderms. Insight into biomineralization has arisen from embryology [25,36], gene sequences and genomic arrangements [14,35,37], the localization and function of protein matrix molecules [24,37,38] and mineral elements [21,37–39], as well as the role of the cellular environment [11,21]. Comparative studies are necessary to rigorously reject the hypothesis that hemichordate and echinoderm ossicles are homologous, and that the regulatory developmental toolkit (if not biominerals *per se*) were present in the ancestral deuterostome.

An understanding of how, when and where minerals are deposited during hemichordate development and what proteins those minerals contain is central to understanding deuterostome skeletal evolution and the problem seems accessible.

Supported by NSERC Discovery Grants to C.B.C. and C.D.B. C.D.B. was supported by a NSERC Discovery Grant to Brian Hall (Dalhousie University) during the early stages of this work. We thank the director of the Darling Marine laboratory for providing facilities (C.B.C.). Patricia Scallion and Dan MacDonald (Dalhousie University) and Truis Smith-Palmer (Chemistry, Saint Francis Xavier University) provided expert assistance with SEM, X-ray microprobe and confocal Raman spectroscopy, respectively. The authors declare no conflict of interest.

REFERENCES

1 Culver, S. J., Pojeta Jr, J. & Repetski, J. E. 1988 First record of Early Cambrian shelly microfossils from west Africa. *Geology* **16**, 596–599. (doi:10.1130/0091-7613(1988)016<0596:FROECS>2.3.CO;2)
2 Cohen, P. A., Schopf, J. W., Butterfield, N. J., Kudryavtsev, A. B. & Macdonald, F. A. 2011 Phosphate biomineralization in mid-Neoproterozoic protists. *Geology.* **39**, 539–542. (doi:10.1130/G131833.1)
3 Smith, A. B. 1990 Biomineralization in echinoderms. In *Skeletal biomineralization: patterns, processes, and evolutionary trends* (ed. J. G. Carter), pp. 413–443. New York, NY: Van Nostrand Reinhold.
4 Wilt, F. H. 2005 Developmental biology meets materials science: morphogenesis of biomineralized structures. *Dev. Biol.* **280**, 15–25. (doi:10.1016/j.ydbio.2005.01.019)
5 Cohen, A. & McConnaughey, T. A. 2003 Geochemical perspectives on coral mineralization. *Rev. Mineral. Geochem.* **54**, 151–187. (doi:10.2113/0540151)
6 Berman, A., Addadi, L., Kvick, Å., Leiserowitz, L., Nelson, M. & Weiner, S. 1990 Intercalation of sea urchin proteins in calcite: study of a crystalline composite material. *Science* **250**, 664–667. (doi:10.1126/science.250.4981.664)
7 Falini, G., Albeck, S., Weiner, S. & Addadi, L. 1996 Control of aragonite or calcite polymorphism by mollusk shell macromolecules. *Science* **271**, 67–69. (doi:10.1126/science.271.5245.67)
8 Aizenberg, J., Tkachenko, A., Weiner, S., Addadi, L. & Hendler, G. 2001 Calcitic microlenses as part of the photoreceptor system in brittlestars. *Nature* **412**, 819–822. (doi:10.1038/35090573)
9 Raz, S., Hamilton, P. C., Wilt, F. H., Weiner, S. & Addadi, L. 2003 The transient phase of amorphous calcium carbonate in sea urchin larval spicules: the involvement of proteins and magnesium ion in its formation and stabilization. *Adv. Funct. Mater.* **13**, 480–486. (doi:10.1002/adfm.200304285)
10 Lambert, G., Lambert, C. C. & Lowenstam, H. A. 1990 Protochordate biomineralization. In *Skeletal biomineralization: patterns, processes, and evolutionary trends* (ed. J. G. Carter), pp. 461–469. New York, NY: Van Nostrand Reinhold.
11 Smith, A. B. 2005 The pre-radial history of echinoderms. *Geol. J.* **40**, 255–280. (doi:10.1002/gj.1018)
12 Bottjer, D. J., Davidson, E. H., Peterson, K. J. & Cameron, R. A. 2006 Paleogenomics of echinoderms. *Science* **314**, 956–960. (doi:10.1126/science.1132310)
13 Ettensohn, C. A. 2009 Lessons from a gene regulatory network: echinoderm skeletogenesis provides insights into evolution, plasticity and morphogenesis. *Development* **136**, 11–21. (doi:10.1242/dev.023564)
14 Livingston, B. T. *et al.* 2006 A genome-wide analysis of biomineralization-related proteins in the sea urchin *Strongylocentrotus purpuratus*. *Dev. Biol.* **300**, 335–348. (doi:10.1016/j.ydbio.2006.07.047)
15 Wilt, F. H., Killian, C. E. & Livingston, B. T. 2003 Development of calcareous skeletal elements in invertebrates. *Differentiation* **71**, 237–250. (doi:10.1046/j.1432-0436.2003.7104501.x)
16 Agassiz, A. 1873 The history of *Balanoglossus* and tornaria. *Am. Acad. Arts Sci. Mem.* **9**, 421–436, 423 plates. (doi:10.2307/25058009)
17 van der Horst, C. J. 1939 Hemichordata. In *Klassen und Ordnungen des Tier-Reichs Vieter Band: Vermes*. (ed. H. G.

Bronn), Band 4, Abt. 4, Buch 2, Tiel 2. p. 737. Leipzig, Germany: Akademische Verlagsgesellschaft.
18 Spengel, J. W. 1903 Neue Beiträge zur Kenntniss der Enteropneusten. I. *Ptychodera flava* Eschsch. Von Laysan. Zoologischn Jahrbüchern, Abtheilung für Anatomie und Ontogenie der Thiere. *Heft* **2**, 271–326 (29 plates).
19 Okazaki, K. & Inoué, S. 1976 Crystal property of the larval sea urchin spicule. *Dev. Growth Differ.* **18**, 413–434. (doi:10.1111/j.1440-169X.1976.00413.x)
20 Massin, C., Mercier, A. & Hamel, J.-F. 2000 Ossicle change in *Holothuria scabra* with a discussion of ossicle evolution within the Holothuroidae (Echinodermata). *Acta Zool.* **81**, 77–91. (doi:10.1046/j.1463-6395.2000.00039.x)
21 Märkel, K. & Röser, U. 1985 Comparative morphology of echinoderm calcified tissues: histology and ultraoid scales. *Zoomorphology* **105**, 197–207. (doi:10.1007/BF00312157)
22 Guss, K. A. & Ettensohn, C. A. 1997 Skeletal morphogenesis in the sea urchin embryo: Regulation of primary mesenchyme gene expression and skeletal rod growth by ectoderm-derived cues. *Development* **124**, 1899–1908.
23 Dandeu, A., Humbert, B., Carteret, C., Muhr, H., Plasari, E. & Bossoutrot, J. M. 2006 Raman spectroscopy—a powerful tool for the quantitative determination of the composition of polymorph mixtures: application to $CaCO_3$ polymorph mixtures. *Chem. Eng. Technol.* **29**, 221–225. (doi:10.1002/ceat.200500354)
24 Mann, K., Wilt, F. H. & Poustka, A. J. 2010 Proteomic analysis of sea urchin (*Strongylocentrotus purpuratus*) spicule matrix. *Proteome Sci.* **8**, 1–12. (doi:10.1186/1477-5956-8-1)
25 Illies, M. R., Peeler, M. T., Dechtiaruk, A. M. & Ettensohn, C. A. 2002 Identification and developmental expression of new biomineralization proteins in the sea urchin *Strongylocentrotus purpuratus*. *Dev. Genes Evol.* **212**, 419–431. (doi:10.1007/s00427-002-0261-0)
26 Ingersoll, E. P. & Wilt, F. H. 1998 Matrix metalloproteinase inhibitors disrupt spicule formation by primary mesenchyme cells in the sea urchin embryo. *Dev. Biol.* **196**, 95–106. (doi:10.1006/dbio.1998.8857)
27 Love, A. C., Andrews, M. E. & Raff, R. A. 2007 Gene expression patterns in a novel animal appendage: the sea urchin pluteus arm. *Evol. Dev.* **9**, 51–68. (doi:10.1111/j.1525-142X.2006.00137.x)
28 Tong, H., Ma, W., Wang, L., Wan, P., Hu, J. & Cao, L. 2004 Control over the crystal phase, shape, size and aggregation of calcium carbonate via a l-aspartic acid inducing process. *Biomaterials* **25**, 3923–3929. (doi:10.1016/j.biomaterials.2003.10.038)
29 Taylor, P. D., Kudryavstev, A. B. & Schoph, J. W. 2008 Calcite and aragonite distributions in the skeletons of bimineralic bryozoans as revealed by Raman spectroscopy. *Invert. Biol.* **127**, 87–97. (doi:10.1111/j.1744-7410.2007.00106.x)
30 Leaf, D. S., Anstrom, J. A., Chin, J. E., Harkey, M. A., Showman, R. M. & Raff, R. A. 1987 Antibodies to a fusion protein identify a cDNA clone encoding msp130, a primary mesenchyme-specific cell surface protein of the sea urchin embryo. *Dev. Biol.* **121**, 29–40. (doi:10.1016/0012-1606(87)90135-7)
31 Farach-Carson, M. C., Carson, D. D., Collier, J. L., Lennarz, W. J., Park, H. R. & Wright, G. C. 1989 A calcium-binding, asparagine-linked oligosaccharide is involved in skeleton formation in the sea urchin embryo. *J. Cell Biol.* **109**, 1289–1299. (doi:10.1083/jcb.109.3.1289)
32 Kazmierczak, J. & Pszczolkowski, A. 1969 Burrows of Enteropneusta in the Muschelkalk (Mid. Trias) of the Holy Cross Mountains, Poland. *Acta Paleontol. Pol.* **14**, 299–324.
33 Cameron, C. B., Swalla, B. J. & Garey, J. R. 2000 Evolution of the chordate body plan: New insights from phylogenetic analysis of deuterostome phyla. *Proc. Natl Acad. Sci. USA* **97**, 4469–4474. (doi:10.1073/pnas.97.9.4469)
34 Cannon, J. T., Rychel, A. L., Eccleston, H., Halanych, K. M. & Swalla, B. J. 2009 Molecular phylogeny of Hemichordata, with updated status of deep-sea enteropneusts. *Mol. Phylogenet. Evol.* **52**, 17–24. (doi:10.1016/j.ympev.2009.03.027)
35 Lowe, C., Wu, M., Salic, A., Evans, L., Lander, E., Stange-Thomann, N., Gruber, C. E., Gerhart, J. & Kirschner, M. 2003 Anteroposterior patterning in hemichordates and the origins of the chordate nervous system. *Cell* **113**, 853–865. (doi:10.1016/S0092-8674 (03)00469-0)
36 Angerer, L. M. & Angerer, R. C. 2003 Patterning the sea urchin embryo: Gene regulatory networks, signaling pathways and cellular interactions. *Curr. Top. Dev. Biol.* **53**, 159–198. (doi:10.1016/S0070-2153(03)53005-8)
37 Melvin, J. G. 2006 Bone: nature of the calcium phosphate crystals and cellular, structural, and physical chemical mechanisms in their formation. *Rev. Mineral. Geochem.* **64**, 223–282. (doi:10.2138/rmg.2006.64.8)
38 Killian, C. E. & Wilt, F. H. 1996 Characterization of the proteins comprising the integral matrix of *Strongylocentrotus purpuratus* embryonic spicules. *J. Biol. Chem.* **271**, 9150–9159. (doi:10.1074/jbc.271.15.9150)
39 Beniash, E., Aizenberg, J., Addadi, L. & Weiner, S. 1997 Amorphous calcium carbonate transforms into calcite during sea urchin larval spicule growth. *Proc. R. Soc. Lond. B* **264**, 461–465. (doi:10.1098/rspb.1997.0066)